Mon. Not. R. Astron. Soc. **000**, 1–15 (2012) Printed 22 April 2013 (MN LATEX style file v2.2)

The ACS LCID Project. VIII. The short-period Cepheids of Leo A⋆

Edouard J. Bernard,[1]† Matteo Monelli,[2,3] Carme Gallart,[2,3] Giuliana Fiorentino,[4] Santi Cassisi,[5] Antonio Aparicio,[2,3] Andrew A. Cole,[6] Igor Drozdovsky,[2,3,7] Sebastian L. Hidalgo,[2,3] Evan D. Skillman,[8] Peter B. Stetson,[9] Eline Tolstoy[10]

[1] *SUPA, Institute for Astronomy, University of Edinburgh, Royal Observatory, Blackford Hill, Edinburgh EH9 3HJ*
[2] *Instituto de Astrofísica de Canarias, Calle Vía Láctea s/n, 38205 La Laguna, Tenerife, Spain*
[3] *Departamento de Astrofísica, Universidad de La Laguna, 38200 Tenerife, Spain*
[4] *INAF-Osservatorio Astronomico di Bologna, via Ranzani 1, 40127 Bologna, Italy*
[5] *INAF-Osservatorio Astronomico di Teramo, via M. Maggini, 64100 Teramo, Italy*
[6] *School of Mathematics & Physics, University of Tasmania, Hobart, Tasmania, Australia*
[7] *Astronomical Institute, St. Petersburg State University, St. Petersburg, Russia*
[8] *Minnesota Institute for Astrophysics, University of Minnesota, Minneapolis, MN 55455, USA*
[9] *NRC Herzberg Institute for Astrophysics, 5071 West Saanich Road, Victoria, BC V9E 2E7, Canada*
[10] *Kapteyn Astronomical Institute, University of Groningen, Groningen, Netherlands*

Accepted 2013 April 16. Received 2013 April 1; in original form 2012 December 29

ABSTRACT

We present the results of a new search for variable stars in the Local Group dwarf galaxy Leo A, based on deep photometry from the Advanced Camera for Surveys onboard the *Hubble Space Telescope*. We detected 166 bona fide variables in our field, of which about 60 percent are new discoveries, and 33 candidate variables. Of the confirmed variables, we found 156 Cepheids, but only 10 RR Lyrae stars despite nearly 100 percent completeness at the magnitude of the horizontal branch. The RR Lyrae stars include 7 fundamental and 3 first-overtone pulsators, with mean periods of 0.636 and 0.366 day, respectively. From their position on the period-luminosity (PL) diagram and light-curve morphology, we classify 91, 58, and 4 Cepheids as fundamental, first-overtone, and second-overtone mode Classical Cepheids (CC), respectively, and two as population II Cepheids. However, due to the low metallicity of Leo A, about 90 percent of the detected Cepheids have periods shorter than 1.5 days. Comparison with theoretical models indicate that some of the fainter stars classified as CC could be Anomalous Cepheids. We estimate the distance to Leo A using the tip of the RGB (TRGB) and various methods based on the photometric and pulsational properties of the Cepheids and RR Lyrae stars. The distances obtained with the TRGB and RR Lyrae stars agree well with each other while that from the Cepheid PL relations is somewhat larger, which may indicate a mild metallicity effect on the luminosity of the short-period Cepheids. Due to its very low metallicity, Leo A thus serves as a valuable calibrator of the metallicity dependencies of the variable star luminosities.

Key words: Cepheids – stars: variables: RR Lyrae – galaxies: individual: Leo A dIrr – Local Group – galaxies: stellar content

1 INTRODUCTION

Classical Cepheids (CC) are the prime distance estimators in the nearby universe thanks to the Leavitt (1908) law, which relates their brightness and period. However, their use is complicated by the existence of other types of Cepheids with different luminosities at a given period: population II Cepheids (P2C) and Anomalous Cepheids (AC). While the

⋆ Based on observations made with the NASA/ESA *Hubble Space Telescope*, obtained at the Space Telescope Science Institute, which is operated by the Association of Universities for Research in Astronomy, Inc., under NASA contract NAS5-26555. These observations are associated with program 10590.

† E-mail: ejb@roe.ac.uk

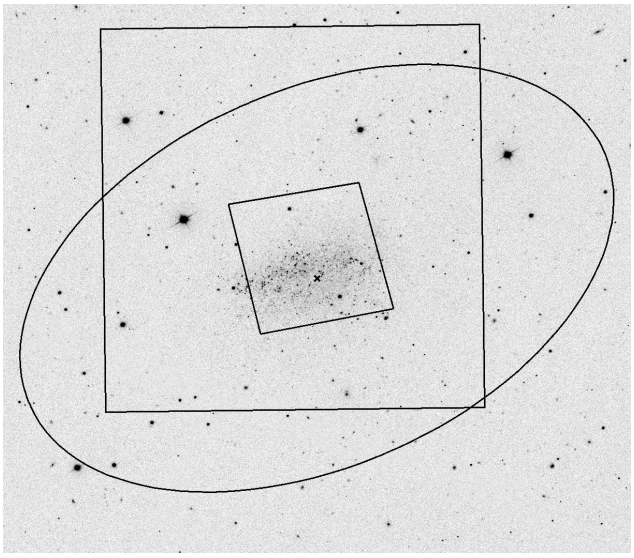

Figure 1. Sloan Digital Sky Survey image of Leo A. The cross and ellipse indicate the center and extent of the galaxy (R.A.=$09^h59^m24.0^s$, decl.=$30°44'47''$, $r = 8'$; Vansevičius et al. 2004), while the small and large squares show the location of our field-of-view and that of Dolphin et al. (2002), respectively.

former have periods similar to those of CC (from less than a day to more than 100 days), they are typically fainter at a given period (∼1−2 mag) such that recognizing CC and P2C is usually straightforward. On the other hand, AC are only slightly fainter than short-period CC (see, e.g. Bono et al. 1997, for a discussion of their formation and evolution). This confusion is even more significant for metal-poor galaxies, in which most of the CC have periods similar to AC (∼0.4−3 days; e.g. IC 1613, Sextans A, Phoenix: Dolphin et al. 2001, 2003; Gallart et al. 2004; Bernard et al. 2010).

An increasing number of studies also suggest that there may be a metallicity effect on the slope and/or zero-point of the period-luminosity (PL) relations (e.g. Sakai et al. 2004; Romaniello et al. 2008; Sandage, Tammann, & Reindl 2009; Bono et al. 2010; Storm et al. 2011), which would affect the distance measurements of galaxies for which metallicity is not well constrained. It is therefore essential to obtain complete surveys of Cepheids in a sample of metal-poor galaxies in order to gain a better understanding of their physical and evolutionary properties.

Leo A, a small star forming dwarf galaxy discovered by Zwicky (1942) and located about 790 kpc away (e.g. Dolphin et al. 2002, hereinafter D02), is among the most metal-poor galaxies of the Local Group (LG). Its current metallicity is A_O=12+log(O/H)=7.30±0.05 (i.e. [Fe/H] ∼ −1.5, or ∼3% solar assuming $A_{O,\odot}$=8.87±0.07; Grevesse & Noels 1993) from the spectroscopy of three H II regions and a planetary nebula (Skillman, Kennicutt, & Hodge 1989; van Zee, Skillman, & Haynes 2006). Tolstoy et al. (1998) drew attention to the relative lack of an ancient stellar population in Leo A, and this was supported by the discovery of the rarity of RR Lyrae stars by D02.

Table 1. Summary of Observations.

Date	UT Start	MHJD[a]	Filter	Exp. Time (s)
2005-12-26	08:45:32	53730.369406	F475W	1200
2005-12-26	09:07:48	53730.384869	F475W	1200
2005-12-26	10:18:55	53730.434371	F814W	1220
2005-12-26	10:41:31	53730.450066	F814W	1220
2005-12-26	19:56:55	53730.835645	F475W	1200
2005-12-26	20:19:11	53730.851108	F475W	1200
2005-12-26	21:30:18	53730.900610	F814W	1220
2005-12-26	21:52:54	53730.916305	F814W	1220
2005-12-28	19:54:20	53732.833851	F475W	1200
2005-12-28	20:16:36	53732.849314	F475W	1200
2005-12-28	21:27:43	53732.898816	F814W	1220
2005-12-28	21:50:19	53732.914510	F814W	1220
2005-12-30	13:28:07	53734.565643	F475W	1200
2005-12-30	13:50:23	53734.581106	F475W	1200
2005-12-30	15:01:31	53734.630619	F814W	1220
2005-12-30	15:24:07	53734.646314	F814W	1220
2005-12-31	21:25:43	53735.897307	F475W	1200
2005-12-31	21:47:59	53735.912770	F475W	1200
2005-12-31	22:59:50	53735.962781	F814W	1220
2005-12-31	23:22:26	53735.978476	F814W	1220
2006-01-02	19:47:55	53737.829384	F475W	1200
2006-01-02	20:10:11	53737.844847	F475W	1200
2006-01-02	21:21:19	53737.894361	F814W	1220
2006-01-02	21:43:55	53737.910055	F814W	1220
2006-01-05	18:07:35	53740.759696	F475W	1200
2006-01-05	18:29:51	53740.775159	F475W	1200
2006-01-05	19:42:00	53740.825379	F814W	1220
2006-01-05	20:04:36	53740.841073	F814W	1220
2006-01-08	13:15:26	53743.556798	F475W	1200
2006-01-08	13:37:42	53743.572261	F475W	1200
2006-01-08	14:49:42	53743.622376	F814W	1220
2006-01-08	15:12:18	53743.638071	F814W	1220

[a] Modified Heliocentric Julian Date of mid-exposure: HJD−2,400,000.

Leo A has been observed as part of the LCID[1] project, which aims at constraining the star formation histories (SFH) of a sample of isolated LG galaxies based on deep color-magnitude diagrams (CMD) and time series photometry obtained with the Advanced Camera for Surveys onboard the *Hubble Space Telescope* (*HST*). The global SFH of Leo A has been presented in Cole et al. (2007), while the analysis of population gradients and spatially resolved SFH will appear in a forthcoming paper (S. Hidalgo et al. 2013, in preparation). Here we present the search for short-period variable stars, in particular Cepheids, for which these data are particularly well suited.

The paper is organized as follows: the data acquisition, reduction, and calibration are summarized in Section 2. We describe the identification of variable stars and their spatial distribution in Section 3. Sections 4 to 6 present the properties of the variable stars and candidate variables detected. The distance estimates based on various tracers and methods are presented in Section 7, and we discuss the implications of our results in Section 8. In Section 9 we summarize our results and present our conclusions.

[1] Local Cosmology from Isolated Dwarfs: http://www.iac.es/project/LCID/.

2 OBSERVATIONS AND DATA REDUCTION

The observations of Leo A were carried out with the ACS onboard the *HST* between 2005 December 26 and 2006 January 8. The observed field was slightly offset from the center of the galaxy, as shown in Figure 1, to cover a longer radial baseline and study possible stellar population gradients. Sixteen *HST* orbits were devoted to this galaxy in two bands (F475W and F814W). Each orbit was split into two ∼1200 second exposures of a given band. This resulted in 16 images per band, for a total exposure time of 19,200 and 19,520s in F475W and F814W, respectively. The complete observing log is presented in Table 1.

We note that the temporal sampling for this galaxy is not as optimal as was the case in the previous papers of this series. In our study of variable stars in Cetus and Tucana (Bernard et al. 2009, hereinafter Paper I) and IC 1613 (Bernard et al. 2010, hereinafter Paper II), we had 25, 32, and 24 datapoints per band, respectively, compared to only 16 here. In addition, the observing strategy for these three galaxies provided alternating observations in F475W and F814W, and therefore observations in a given filter that were well separated in time. For Leo A, the paired observations in a given band are only 22 minutes apart, thus limiting their utility. While it did not affect our ability to detect candidate variables, some light curves have gaps which could limit the accuracy of the measured mean magnitudes (see Section 5).

The DAOPHOT/ALLFRAME suite of programs (Stetson 1994) was used to obtain the instrumental photometry of the stars on the individual, non-drizzled images provided by the *HST* pipeline. Additionally, we used the pixel area maps and data quality masks to correct for the pixel area variation and to flag bad pixels. Standard calibration was carried out as described in Sirianni et al. (2005). We refer the reader to Monelli et al. (2010) for a detailed description of the data reduction and calibration. The final CMD is presented in Figure 2, where the $(F475W + F814W)/2 \sim V$ filter combination was chosen for the ordinate axis so that the horizontal-branch (HB) appears approximately horizontal.

The light-curves of the variable stars were then converted to Johnson-Cousins BVI magnitudes using the transformations given Paper I. As we have shown Paper II from the comparison of the light curves of Cepheids in common between our HST survey and OGLE[2], these transformations can be safely used to analyse the properties (e.g. magnitude and amplitude) of the variable stars.

3 VARIABLE STARS

3.1 Identification and period search

The candidate variables were extracted from the photometric catalogs using the variability index of Welch & Stetson (1993); this process yielded ∼700 candidates. A preliminary check of the light-curve and position on the CMD, together with a careful inspection of the stacked image, allowed us to discard false detections due to cosmic-ray hits, chip defects

[2] Optical Gravitational Lensing Experiment: http://ogle.astrouw.edu.pl/

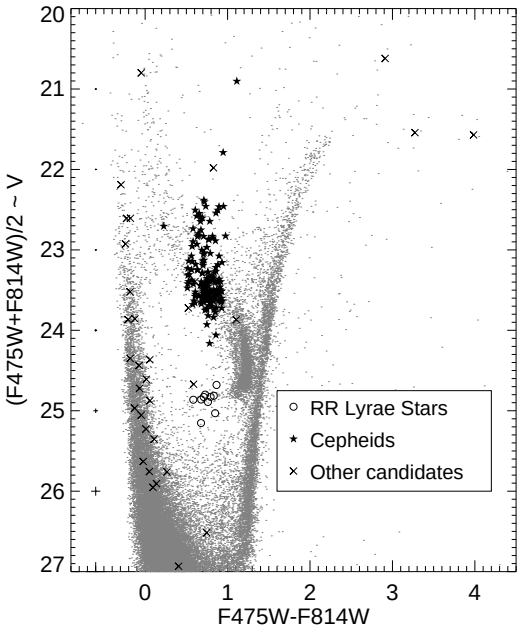

Figure 2. Color-magnitude diagram of Leo A from our ACS data. The variables are overplotted as labeled in the inset.

or stars located under the wings of bright stars. Our final catalogue contains 166 bona fide variables and 33 candidates for which we could not determine a period (e.g. main-sequence and red giant branch [RGB] variables, eclipsing binaries). The variables and candidates are shown overplotted on the CMD in Figure 2 using their intensity-averaged mean magnitudes. The individual F475W and F814W measurements for all the variables and candidates, as well as the transformed BVI magnitudes, are listed in Table 2.

The period search was performed through Fourier analysis (Horne & Baliunas 1986) taking into account the information from both bands simultaneously, then refined interactively by modifying the period until a tighter light curve was obtained. For each variable, datapoints with error bars larger than 3-σ above the mean error bar size were rejected through sigma clipping with five iterations. The periods are given with three significant figures only to reflect the sparse sampling of the light curves. Note that for the same reason, some of the periods may be aliases of the true periods.

The classification of the candidates was based on their light curve morphology and position in the CMD. We found a large number of Cepheids but very few RR Lyrae stars (156 and 10, respectively), in very good agreement with the study of D02. The small number of RR Lyrae stars – which is not due to incompleteness, our photometry being near 100 percent complete at the magnitude of the HB – is not surprising considering the SFH of Leo A (Cole et al. 2007, S. Hidalgo et al. 2013, in preparation), which shows a very low star formation rate for the earliest epochs. To obtain the amplitudes and intensity-averaged magnitudes of the variables, we fitted the light curves with a set of templates based on the set of Layden et al. (1999, see Paper I).

Table 3 summarizes the properties of the bona fide variable stars in our final catalogue. The first two columns give the identification number and type of variability, while the

Table 2. Photometry of the Variable and Candidate Variable Stars. The complete table is available from the online edition.

MHJD[a]	F475W	σ_{475}	B[c]	σ_B	MHJD[b]	V[c]	σ_V	MHJD	F814W	σ_{814}	I[c]	σ_I
V001												
53730.369406	25.296	0.030	25.442	0.030	53730.401888	24.978	0.030	53730.434371	24.370	0.061	24.356	0.061
53730.384869	25.284	0.056	25.418	0.056	53730.417468	24.986	0.056	53730.450066	24.416	0.036	24.400	0.036
53730.835645	25.181	0.032	25.311	0.032	53730.868127	24.889	0.032	53730.900610	24.330	0.034	24.314	0.034
53730.851108	25.239	0.048	25.385	0.048	53730.883706	24.921	0.048	53730.916305	24.314	0.033	24.300	0.033
53732.833851	25.107	0.031	25.238	0.031	53732.866334	24.813	0.031	53732.898816	24.252	0.036	24.236	0.036

[a] Modified HJD of mid-exposure: HJD−2,400,000.
[b] Midpoint of F475W and F814W MHJD.
[c] Transformed from the F475W and F814W magnitudes using the equations of Paper I.

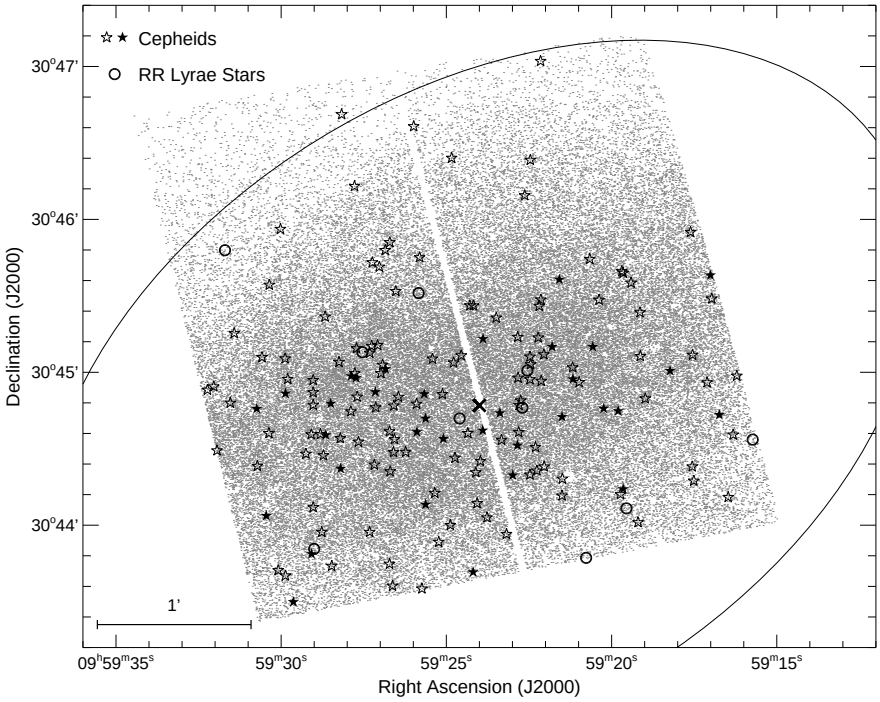

Figure 3. Spatial distribution of stars in our observed field, where the variables are overplotted as labeled in the inset. The cross and ellipse represent the center and Holmberg radius of Leo A (3.5′; Vansevičius et al. 2004).

next two list the equatorial coordinates (J2000.0). Columns (5) and (6) give the period and logarithm of the period, in days. The intensity-averaged mean magnitudes $\langle F475W \rangle$ and $\langle F814W \rangle$, and color $\langle F475W \rangle - \langle F814W \rangle$ are given in columns (7), (9), and (11). The amplitudes in the F475W and F814W bands measured from the template fits are listed in columns (8) and (10). The last six columns alternately list the intensity-averaged mean magnitudes and amplitudes in the Johnson B, V, and I bands. For the candidate variables, we only list the coordinates and approximate magnitudes in Table 4.

3.2 Spatial Distribution

Figure 3 presents the spatial distribution of stars in our field-of-view (FOV), where the RR Lyrae stars (open circles) and Cepheids (open and filled stars) are shown. The cross and ellipse represent the center and Holmberg radius of Leo A (3.5′, from Vansevičius et al. 2004). Despite their small number, the RR Lyrae stars seem to be roughly uniformly distributed over the field. On the other hand, the Cepheids are mostly located close to the center of the galaxy, where the main sequence stars are strongly concentrated (D02, S. Hidalgo et al. 2013, in preparation). This shows that star formation in the past ∼1 Gyr was confined to the central region of the galaxy.

We further separated the Cepheids into a bright sample and a faint sample, with a division at W_{814}=22 (see Section 5). These samples are shown as filled and open stars, respectively. Interestingly, the Cepheids of the bright sample are even more concentrated close to the center of the galaxy than the whole sample, all of them being located in

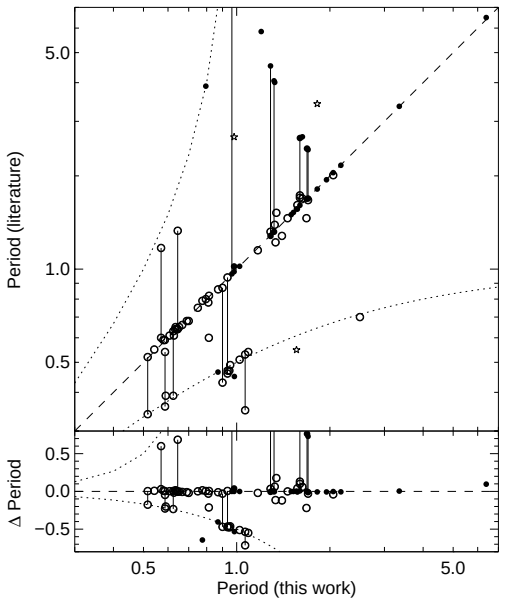

Figure 4. Period difference for the variable stars in common between this and previous works: D02 (open circles), G07 (filled circles), and H94 (open stars). When two periods were listed for a given star, these are joined by vertical lines. The dashed line is the identity line, and the dotted lines represent the one-day aliases of the best period.

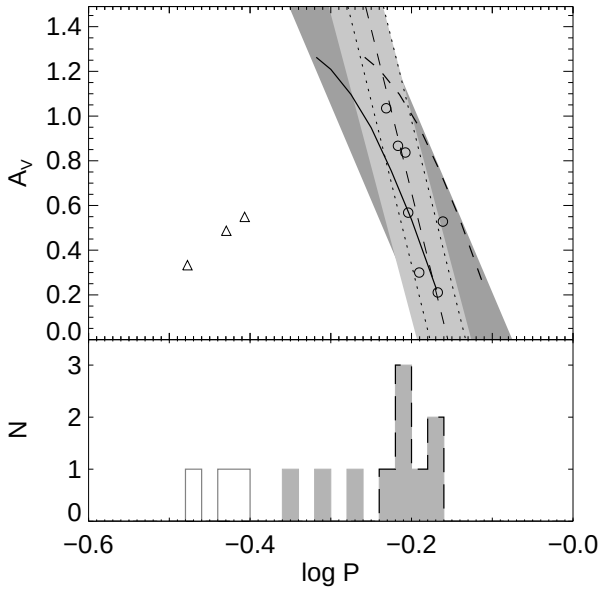

Figure 5. Top: Period-amplitude diagram for the RR Lyrae stars. Circles and triangles represent RR*ab* and RR*c*, respectively. The thin dashed line is a fit to the period-amplitude of the RR*ab*; the dotted lines show the 1.5-σ limits. The light and dark grayed areas represent the $\pm$1.5-σ limits of Cetus and Tucana, respectively, from Paper I. The solid and dashed curved lines show the loci of OoI and OoII globular clusters from Cacciari, Corwin, & Carney (2005). Bottom: Period histogram for the RR Lyrae stars of the top panel. RR*ab* and RR*c* are shown as the black dashed and solid gray lines, respectively, while the filled histogram represent the fundamentalized RR Lyrae stars.

the lower half of our FOV. These gradients indicate that the star forming region has been shrinking with time (see e.g. Hidalgo et al. 2009), at least in the past Gyr or so. This result is in excellent agreement with the SFH as a function of galactocentric radius of S. Hidalgo et al. (2013, in preparation).

3.3 Comparison with previous catalogues

The search for variable stars in Leo A has been carried out by several authors prior to this work. We cross-matched the catalogues from the literature with ours to identify the stars in common and compare the measured properties. These are listed in Table A1. We give their index, type, and period measured from our data, together with their identifications and periods from previous catalogues[3].

Variable stars in Leo A were first mentioned by Sandage (1986). While the data were not sufficient for a detailed study, Sandage found eight candidates by blinking three plate pairs. However, only the four best candidates are labeled on the finding chart, and no information on periods or magnitudes are given. By comparing his finding charts with ours, we found the following: his "definite variable" (RA=09:59:19.52, Dec=+30:44:13.4) is a very bright MS star; one candidate (RA=09:59:28.88, Dec=+30:45:42.6) is a blend of two relatively bright RGB stars, and another (RA=09:59:24.70, Dec=+30:44:48.1) is close to the tip of the RGB (TRGB); none of these appear to be variable in our data, possibly due to having periods longer than our observational baseline. The fourth candidate is out of our FOV, but corresponds to the D02 Cepheid C2-V67.

The first actual search for variable stars was carried out by Hoessel et al. (1994, hereinafter H94) using data from a variety of telescopes and instruments, from which they discovered 14 suspected variables (including five Cepheids: V5, V8, V9, V10, and V14 in their catalogue). Out of these, V1, V2, and V14 are located outside of our FOV. The stars V3–V6, V8, and V12 are not variables in our data, and V11 is a long-period variable (LPV). We classify the remaining four candidates (V7, V9, V10, V13) as Cepheids, but the periods from H94 cannot phase our data.

More recently, D02 analysed 28 images (23 in V, five in R) taken with the WIYN 3.5-m telescope, and found 92 candidates variables (84 Cepheids and 8 RR Lyrae stars). Our catalogue contains 49 of the 50 variables in our FOV. Their C2-V33 appears to be a (non-variable) red clump (RC) star in our data. As shown in Figure 4, for most of the stars in common we find a very good agreement between their reported periods and ours. For the few variables with discrepant periods, we checked that their value did not give a better light curve. The dotted lines in Figure 4 show that most of the inadequate periods of D02 are due to the one-day aliasing usually affecting ground-based data.

The most recent work on variable stars in this galaxy is by the Munich group (Snigula 2006; Gössl, Snigula, & Hopp 2006; Gössl 2007, hereinafter G07) using small telescopes

[3] The J2000.0 coordinates of all the variable star candidates from Sandage (1986), Hoessel et al. (1994), and D02, which are not listed in the original publications, are available from the first author on request.

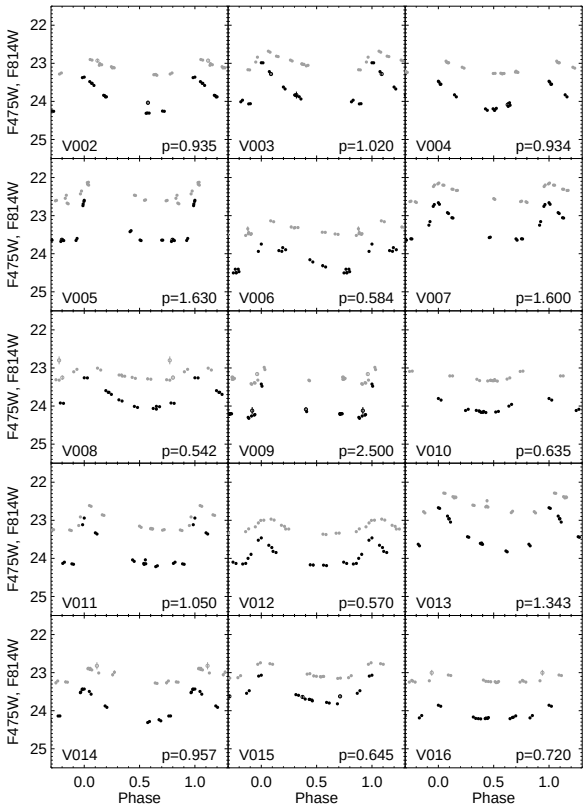

Figure 6. Sample light curves of the Cepheids stars in the $F475W$ (black) and $F814W$ (gray) bands, phased with the period in days given in the lower right corner of each panel. Open symbols show the bad data points, i.e. with errors larger than 3-σ above the mean error of a given star, which were not used in the calculation of the period and mean magnitudes. For a few very bright Cepheids, the light curves have been shifted downward by 1 or 2 mag, as shown by an arrow in the top left corner of a panel. The complete sample of light curves is available in the on-line version.

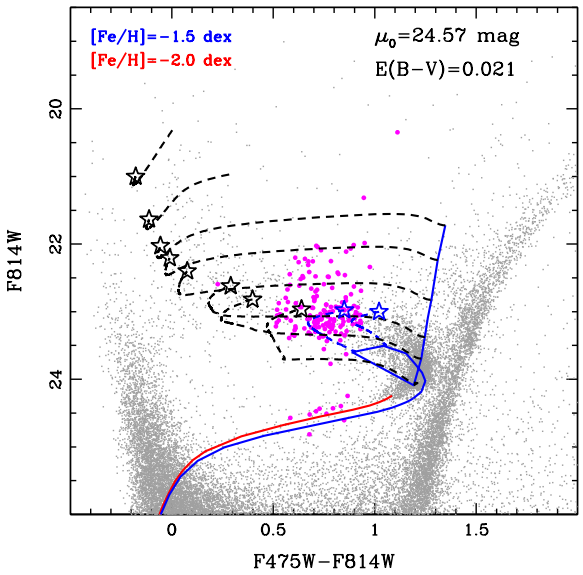

Figure 7. CMD showing the observed variable (magenta filled circles) and non-variable (gray dots) stars, where theoretical predictions from the BaSTI library (Pietrinferni et al. 2004) are overplotted. The thick blue line shows the ZAHeB locus for [Fe/H]=−1.5. Evolutionary tracks for both anomalous (blue dashed lines, M = 2.0 and 2.14 $M_\odot$) and classical (black dashed lines, M = 2.2, 2.4, 2.6, 3.0, 3.5, 4.0, 5.0, and 7.0 $M_\odot$) Cepheids are shown for the same metallicity. The stellar tracks extend from the ZAHeB to the central helium exhaustion, represented by the open star symbols. The thick red line shows the ZAHeB locus for [Fe/H]=−2.0, which provides a much better fit to the old stellar populations of the HB (see Section 8.1).

with the aim of studying the properties of bright variables in a sample of six northern dwarf irregular galaxies, including Leo A. The work of G07 focused on Cepheids while Snigula (2006) concentrated on LPVs, although some of the stars with unsecure classification appear in both. Given the relatively short time baseline of our observations preventing us from detecting long periodicities, most of the previously known stars in our catalogue are in common with G07. In column 7 of Table A1 we use the star indices of G07, where LS, LM, and LL refer to short, medium, and long period variables, with cut-offs at 1 and 10 days, but also list the indices from Gössl, Snigula, & Hopp (2006, starting with V-) and from Snigula (2006, starting with LeoA-), when available.

The catalogue of G07 contains 131 candidate variables with R<23.5 and P<130 days. Of these, 33 are matches to Cepheids in our catalogue, including 19 with periods in good agreement with ours (see Figure 4). The remaining ones are either outside of our FOV (45), or not variable in our data (53). We note, however, that all their candidates flagged as 'best' and 'good' and located in our FOV are indeed Cepheids.

4 RR LYRAE STARS

Ten of the variable stars in our sample are located on the HB and were classified as RR Lyrae stars. From their light curves and periods, we further classify them as 7 fundamental-mode (RRab) and 3 overtone (RRc) pulsators. We find mean periods of 0.636 and 0.366 day for the RRab and RRc, respectively, and a fraction of overtone pulsators of $f_c = N_c/(N_{ab} + N_c) = 0.3$. These numbers place Leo A in the Oosterhoff (1939) type II group, whereas the vast majority of Local Group dwarf galaxies have properties intermediate between those of the type I and type II groups (OoI and OoII, respectively; see Smith, Catelan, & Clementini 2009; Catelan 2009). We note, however, that the reliability of these numbers may be affected by the small number of RR Lyrae stars and suboptimal light curves.

In fact, this classification is not as clear from the location of these variables in the period-amplitude diagram. Figure 5 presents the period-amplitude diagram (*top*) and the period distribution (*bottom*) of the RR Lyrae stars. In the top panel, RRab and RRc are shown as open circles and open triangles, respectively. The solid and dashed curved lines show the loci of OoI and OoII globular clusters from Cacciari, Corwin, & Carney (2005). The low-

amplitude RR*ab* stars seem to lie on the OoI locus, while the ones with higher amplitude are located between the two groups, suggesting a Oosterhoff-intermediate classification instead. The relatively long mean period for the RR*ab* stars may thus be due to the lack of high-amplitude RR*ab* stars.

The shaded areas in the top panel of Figure 5 represent the location of RR*ab* stars in Cetus and Tucana from Paper I. The figure shows that the distribution of the RR*ab* of Leo A in period-amplitude space, forming a tight and almost vertical sequence, is very similar to that of Cetus. On the other hand, in Paper II we found that the RR*ab* in IC 1613 were more similar to those in Tucana. Interestingly, both Cetus and Leo A seem to have had a significantly lower SFR at very early epochs than Tucana and IC 1613, which may partly explain the difference.

The very low number of RR Lyrae stars is a remarkable result given the high stellar density in our FOV and completeness at the magnitude of the HB ($\gtrsim$98 percent). For comparison, we found 90 or more RR Lyrae stars in roughly similar areas in the other LCID galaxies (Paper I; Paper II). To make this comparison more meaningful, for each of these galaxies we calculated the number of RR Lyrae stars relative to the number of RGB stars within the 2.5 magnitudes below the TRGB. We find 0.01, 0.09, 0.58, and 0.81 for Leo A, IC 1613, Cetus, and Tucana, respectively. Assuming RGB and RR Lyrae stars are older than 1.5 and 10 Gyr, respectively, this ratio gives a measure of the fraction of very old stellar population with respect to the intermediate-age and old stellar populations of the galaxy. The extremely low value found for Leo A is in very good agreement with the results of the SFH analysis. Cole et al. (2007) and S. Hidalgo et al. (2013, in preparation) found very little, if any, star formation for ages older than 10 Gyr, and showed that 90 percent of the star formation had occurred more recently than 8 Gyr ago.

5 CEPHEIDS

Most of the variable stars in our sample are found in the classical instability strip above the HB. We present their light curves in Figure 6. Recent work has shown that at the metallicity of the young population of Leo A ([Fe/H] ~ -1.5), CC and AC can occupy a similar region in the CMD (Fiorentino et al. 2012). CC are young, relatively massive stars ($\gtrsim$2.2 $M_\odot$) in the phase of core helium burning. AC, on the other hand, are older and less massive stars on the HB phase of evolution, burning helium in the core in partially degenerate conditions after undergoing the so-called helium flash at the TRGB (e.g. Demarque & Hirshfeld 1975).

In Figure 7 we show a comparison of the observed location of the Cepheids in the CMD with the theoretical predictions for both CC and AC with masses 2.0–7.0 $M_\odot$. The models are based on the BaSTI stellar evolution library (Pietrinferni et al. 2004), and were shifted to the distance and foreground reddening of Leo A. The thick blue line shows the zero-age helium-burning (ZAHeB) locus, which represents the ignition of helium in the core in either degenerate ($M \leqslant 2.14$ $M_\odot$ at [Fe/H] $= -1.5$) or non-degenerate ($M > 2.14$ $M_\odot$) conditions. The black and blue dashed lines show the theoretical tracks for CC and AC, respectively. They extend from the ZAHeB to the open star symbols

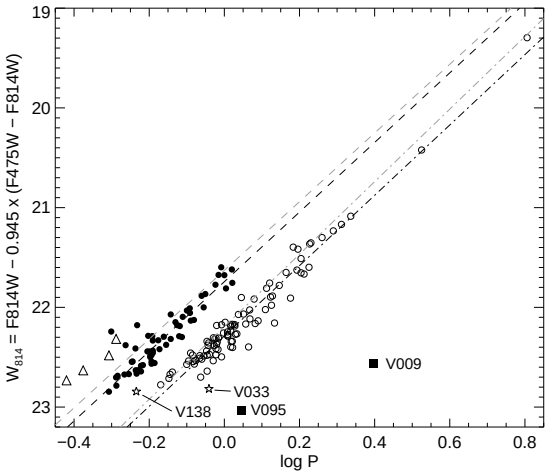

Figure 8. Period-Wesenheit diagram for Cepheids in Leo A. Open circles, filled circles, and open triangles represent fundamental, first overtone, and second overtone pulsators, respectively. A few outliers are labeled and discussed in Section 5. The black dash-dotted and dashed lines are linear fits to the fundamental and FO Cepheids. The gray lines are the same fits to the IC1613 Cepheids (Paper II), shifted to the distance of Leo A.

representing exhaustion of helium in the core. The Figure shows that while all the Cepheids brighter than F814W$\sim$23 are most likely CC, the fainter ones could be a combination of both CC and AC. Note that this result does not change for significantly lower metallicity (i.e. [Fe/H]$=-1.8$). On the other hand, for [Fe/H]$=-1.3$ and higher, the AC tracks do not enter the instability strip, leading to a pure CC population.

Since the various types of Cepheids have different magnitudes at a given period, their locations in the PL diagrams can be used to differentiate their types (e.g., Fiorentino et al. 2006; Monelli et al. 2012). Figure 8 shows the period-luminosity diagram of all the Cepheids in Leo A. Here we used the reddening-free Wesenheit magnitude

$$W_{814} = F814W - 0.945 \times (F475W - F814W)$$

in order to reduce the scatter due to interstellar extinction and the intrinsic dispersion due to the finite width of the instability strip. Despite the sub-optimal sampling of our light curves, the sequences of fundamental (F, open circles) and first-overtone (FO, filled circles) mode Cepheids are very well defined. The black dash-dotted and dashed lines represent linear fits to the F and FO Cepheids, respectively. The grey lines represent similar fits to the IC 1613 variables of Paper II, shifted to the distance of Leo A, and are discussed in Section 7.3. The four Cepheids shown as open triangles, $\sim$0.4 brighter than the FO relation, have sinusoidal light curves with very low amplitudes ($A_{F475W} \lesssim 0.2$ mag, see Figure 6), and are located along the blue edge of the instability strip. We therefore classify them as second-overtone (SO) mode Cepheids. A few outliers are labeled and discussed below. From this plot, we classify 91 and 58 stars as F and FO Cepheids, respectively.

Figure 9 shows the Leo A Cepheids in the period-Wesenheit ($P - W_I$) diagram, together with the OGLE-III Cepheids of the Small and Large Magellanic Clouds (LMC

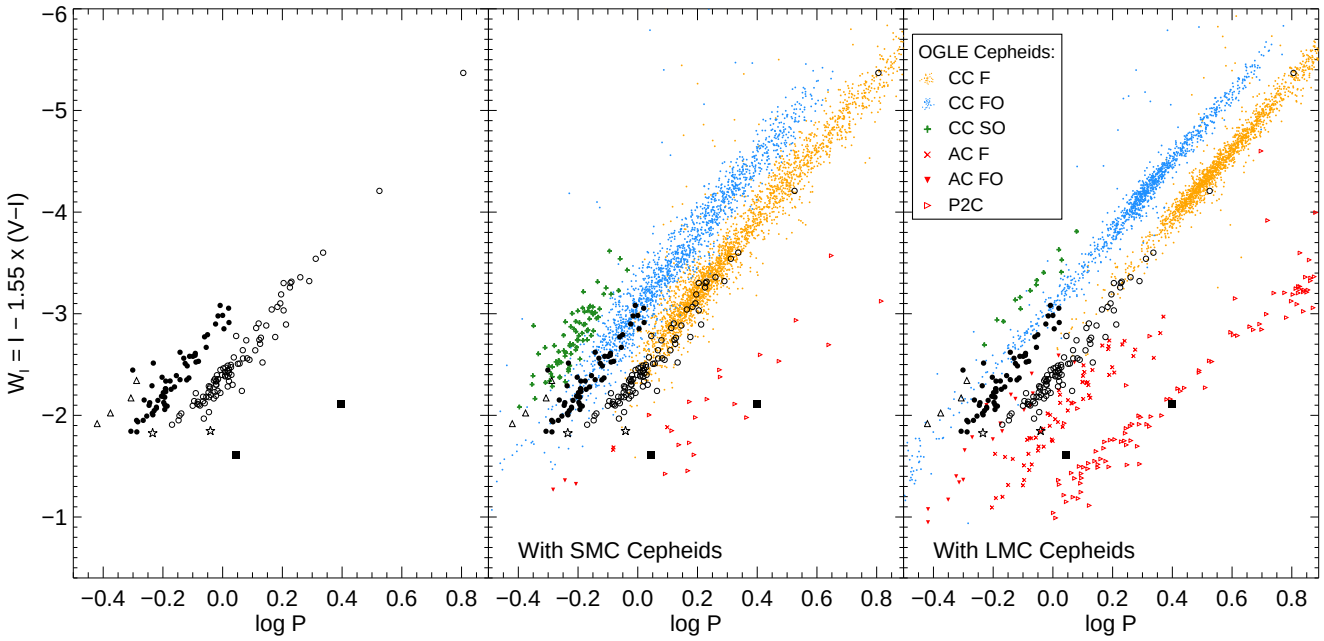

Figure 9. Period-luminosity diagram for Cepheids in Leo A (black symbols as in Figure 8). The left panel shows the Leo A data alone, while in the middle and right panels the Cepheids in the SMC and LMC, respectively, are also shown. In the inset, CC, AC, and P2C stand for classical, anomalous, and population II Cepheids; F, FO, and SO indicate fundamental, first-, and second-overtone mode pulsations.

and SMC, respectively; Soszyński et al. 2008a,b, 2010a,b) in the middle and right panels. In all three panels, the Leo A Cepheids are shown with the same symbols as in Figure 8, and are shown by themselves in the left panel for clarity. The Cepheids of Leo A were shifted according to the TRGB distance determined in Section 7.1, i.e. $(m-M)_0$ =24.57. The LMC/SMC apparent magnitudes were converted to absolute magnitudes assuming a distance modulus of 18.515±0.085 to the LMC (Clementini et al. 2003), and a distance offset of 0.51 of the SMC relative to the LMC (Udalski et al. 1999c). The middle panel shows that the bulk of Leo A Cepheids are in relatively good agreement with the SMC Cepheids – even though the significant spread of the SMC Cepheids complicates the comparison – and extend the F, FO, and SO PL relations to shorter periods and fainter magnitudes. This supports their identification as CC.

We note, however, that at the shortest period the FO Cepheids of Leo A and the SMC seem to be slightly offset, the former appearing ∼0.1 mag fainter than the latter at $\log P \sim -0.25$. This is more obvious in the right panel, which shows that they are fainter by ∼0.2–0.3 mag than the LMC classical Cepheids at a given period. Part of these offsets may be due to uncertainties in the distance moduli used. On the other hand, we also find small differences in the slope of the PL relations calculated by linear regression over the period ranges $-0.2 < \log P < 1.0$ and $-0.4 < \log P < 0.8$ for the F and FO Cepheids, respectively. For the F and FO Cepheids of Leo A, we find slopes of −3.538±0.074 and −3.58±0.15, respectively, comparable to those of the SMC (−3.522±0.013 and −3.639±0.020), but mildly steeper than those of the LMC (−3.332±0.012 and −3.439±0.011). The possible origin of the offset is further discussed in Section 8.

Despite this offset, most of the Leo A Cepheids lie closer to the sequences of F and FO classical Cepheids of the Magellanic Clouds than to the other types of Cepheids (AC and P2C). The Cepheids that were flagged as outliers in Figure 8 fall squarely on the sequences of other types of Cepheids. In particular, the two faint Cepheids with periods longer than 1 day (V009 and V095, filled squares) lie on the P2C sequence of both Magellanic Clouds. V138, shown as an open star, lies between the F and FO classical Cepheids PL, but fits very well with the FO AC of the LMC. Some of the other Cepheids that are slightly offset from the classical F and FO sequences (e.g. V033 in Figure 8) may actually be AC. Unfortunately, our light curves are not sufficiently densely populated to classify the Cepheids based on light curve morphology. The follow-up observations of Fiorentino et al. (2013, in preparation), carried out with the Gemini telescope, may help us to confirm the presence of AC in Leo A thanks to the better sampling.

6 OTHER CANDIDATE VARIABLES

In addition to the classical instability strip variables presented above, we detected another 33 variable candidates (VC) throughout the CMD, for which we could not determine the period because of inadequate temporal sampling or insufficient number of datapoints. They are shown as crosses in the CMD in Figure 2. The majority of these candidate variables are located on the MS or close to the TRGB, and are therefore most likely eclipsing binaries or LPV; two of these (VC11 and VC32) are possible δ-Scuti stars. Their coordinates and approximate magnitudes are provided in Table 4. They are labeled as main-sequences variables (MSV),

Table 3. Pulsational Properties of the Variable Stars. The complete table is available from the online edition.

ID	Type[a]	R.A. (J2000)	Decl. (J2000)	Period (days)	log P (days)	$\langle F475W \rangle$	A_{475}	$\langle F814W \rangle$	A_{814}	$\langle F475W \rangle - \langle F814W \rangle$	$\langle B \rangle$	A_B	$\langle V \rangle$	A
V001	*ab*	09 59 15.73	+30 44 33.6	0.690	-0.161	25.112	0.552	24.246	0.436	0.865	25.211	0.657	24.796	0.5
V002	F	09 59 16.21	+30 44 58.6	0.935	-0.029	23.941	0.964	23.100	0.551	0.841	24.061	1.065	23.669	0.7
V003	F	09 59 16.32	+30 44 35.5	1.02	0.009	23.729	1.186	22.980	0.567	0.750	23.843	1.321	23.473	0.9
V004	F	09 59 16.47	+30 44 11.0	0.934	-0.030	23.572	1.549	23.039	0.621	0.533	23.682	1.678	23.411	1.1
V005	F	09 59 16.74	+30 44 43.3	1.63	0.212	23.263	1.382	22.442	0.459	0.821	23.359	1.615	22.918	1.2

[a] *ab* and *c*: fundamental mode and overtone RR Lyrae star; F, FO, SO: fundamental mode, first-, and second-overtone Classical Cepheid; P2C: population II Cepheid; Cep: Cepheid of unknown type.

classical instability strip variables (ISV), or LPV based on their location on the CMD.

7 DISTANCE TO LEO A

7.1 TRGB Luminosity

In the previous articles of this series (Paper I; Paper II), we used exclusively the properties of the variable stars to obtain the distance to the host galaxy. However, the rather sparse sampling of our light curves, fainter than expected Cepheids, and very low number of RR Lyrae stars in Leo A lead to somewhat uncertain measurements (see below). Therefore, we also include measurement of the distance using the TRGB method (e.g. Da Costa & Armandroff 1990; Lee, Freedman, & Madore 1993; Salaris & Cassisi 1998), for which the dependence on age and metallicity is well understood. In particular, Salaris (2012) has shown that at the low metallicity of Leo A, the luminosity of the TRGB is not affected by age (at least for ages larger than ∼4 Gyr old), metallicity, metal mixture, and helium abundance, and that the empirical and theoretical models agree within ∼0.05 mag.

Figure 10 shows the box used for the selection of RGB stars in the Leo A CMD (top left panel) and corresponding luminosity function (LF, bottom panel). We applied the same method to IC 1613 for comparison with the variable star distance from Paper II and to illustrate the reliability of the method; we show the CMD and LF in the top right and bottom panels, respectively. The open circles in the CMDs represent the Cepheids and RR Lyrae stars. To determine the magnitude of the TRGB, we convolved the LFs with a Sobel kernel of the form [-1,-2,0,2,1]; the filter response function is shown as a dotted line in the bottom panels, and the center of the peak corresponding to the TRGB of each galaxy is indicated by the thick vertical line. We find $F814W_0$ =20.46±0.12 and 20.36±0.09 for the TRGB of Leo A and IC 1613, respectively, shown as the horizontal lines in the top panels. For each galaxy, the errorbars were calculated by measuring the TRGB luminosity of 1000 synthetic CMDs containing the same number of stars in the selection box as the real galaxies; the quoted uncertainty is the standard deviation of these measurements.

The distances were obtained from the TRGB magnitudes using the empirical absolute TRGB magnitude calibrations in the *HST* flight bands from Rizzi et al. (2007). While these contain a color term based on either the F555W or F606W bands, which we do not have for Leo A, the (F555W-F814W) color is very close to (V−I). We can therefore use the TRGB color from ground-based observations. For Leo A and IC 1613, we used $(V-I)_{TRGB}$=1.40±0.05 (Tolstoy et al. 1998) and 1.60±0.02 (Rizzi et al. 2007), respectively. These give distance moduli of $(m-M)_{\rm Leo\ A,0}$ =24.57±0.13 and $(m-M)_{\rm IC\,1613,0}$ =24.44±0.09. The latter value is precisely the same as the distance determined from Cepheids and RR Lyrae stars in Paper II. It shows that the TRGB method used here and the variable stars distance methods of Paper II produce homogeneous and reliable results. We note that using the theoretical TRGB magnitude calibrations from Cassisi & Salaris (2013), which takes into account the updated electron conduction opacities of Cassisi et al. (2007), produces comparable values within the uncertainties ($(m-M)_{\rm Leo\ A,0}$ =24.58±0.13 and $(m-M)_{\rm IC\,1613,0}$ =24.49±0.09). Our TRGB distance to Leo A is also in good agreement with previous determination using this method ($(m-M)_0$ = 24.5±0.2; Tolstoy et al. 1998; Schulte-Ladbeck et al. 2002).

7.2 RR Lyrae Stars

In the previous papers of the series we used both the mean magnitude of the RR Lyrae stars (luminosity–metallicity relation) and the location of the first-overtone blue edge of the instability strip (period–luminosity–metallicity relation) to estimate the distance to the host galaxy. However, the latter method depends on having a sufficiently populated HB within the instability strip, and is thus not applicable here due to the very low number of RR Lyrae stars found in Leo A. Here and in the following section, we used the intensity-averaged mean magnitudes in the Johnson-Cousin bands.

The luminosity–metallicity relation used here was derived in Paper I, and has the form:

$$M_V = 0.866(\pm0.085) + 0.214(\pm0.047)[\mathrm{Fe/H}].$$

The slope was derived by Clementini et al. (2003) from spectroscopy of a large number of RR Lyrae stars in the LMC, while the zero-point was set such that the LMC distance modulus is $(m-M)_{\rm LMC,0}$=18.515±0.085 (Clementini et al. 2003, adopting [Fe/H] = −1.5 for the old LMC population; Gratton et al. 2004).

We find a dereddened mean magnitude for the 10

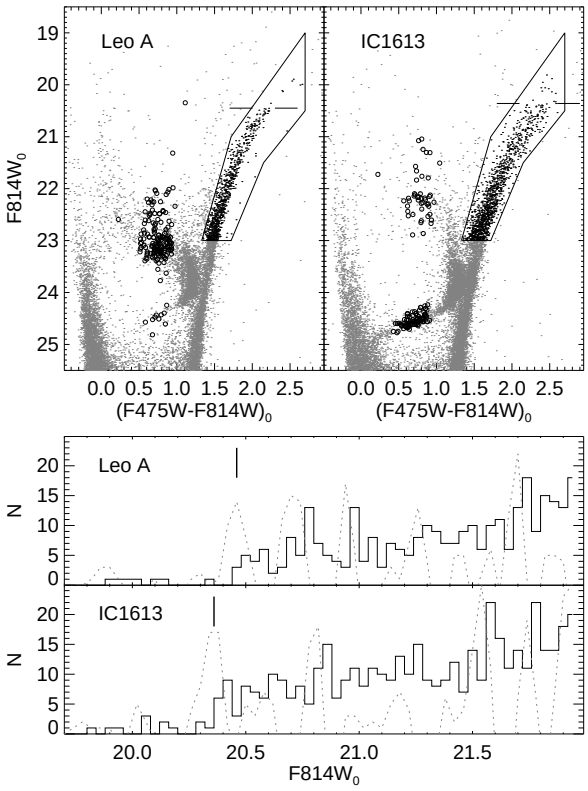

Figure 10. Top panels: CMDs of Leo A (left) and IC 1613 (right), showing the box used for the selection of RGB stars (black points). The open circles represent the Cepheids and RR Lyrae stars, and the magnitude of the TRGB is marked by the horizontal lines near $F814W_0 \sim 20.5$. Bottom panels: Luminosity functions of Leo A and IC 1613 (black histograms). The dotted line represents the Sobel filter response, and the location of the tip is shown by a vertical line.

RR Lyrae stars of $\langle V \rangle_0$=24.916±0.044. The star formation and chemical enrichment history calculated by Hidalgo et al. (2013, in preparation) from CMD fitting gives a mean metallicity of [Fe/H] = −2.0±0.1 for the old population. At this metallicity, the relation given above predicts a HB luminosity of M_V=0.44±0.11. The uncertainty was quantified through Monte-Carlo simulations. This gives a distance modulus of (m−M)$_0$=24.48±0.12 after correcting for reddening. We note that the distance does not change significantly if we exclude the three outlier RR Lyrae stars (one bright and two faint, see Figure 2), which yields (m−M)$_0$=24.44±0.11. This distance is in good agreement with the TRGB distance derived in Section 7.1.

7.3 Cepheid Period-Luminosity(-Color) relations

Given the significant number of F, FO, and SO Cepheids observed in our field and rather well-defined PL sequences (see Figure 8), we can calculate the distance to Leo A using their photometric and pulsational properties. As in Paper II, we used both the $P-W_I$ relations for F and FO Cepheids, and the period-luminosity-color (PLC) relation for SO Cepheids (Bono, Caputo, & Marconi 2001). In addition, we also include the distance estimates using the recent PL relation of Tammann, Reindl, & Sandage (2011), derived specifically for metal-poor galaxies from short-period SMC Cepheids.

The P−W$_I$ relations were derived in Paper II by combining the LMC and SMC Cepheids from the OGLE-II database (Udalski et al. 1999a,b) assuming $\Delta(m - M)_0 = 0.51$ (Udalski et al. 1999c) and an LMC distance modulus of (m−M)$_{\rm LMC,0}$=18.515±0.085 (Clementini et al. 2003). We found

$$W_{I,F} = -3.435(\pm0.007)\ \log\ P_F - 2.540(\pm0.006),$$

$$W_{I,FO} = -3.544(\pm0.013)\ \log\ P_{FO} - 3.067(\pm0.007),$$

for the fundamental and first-overtone Cepheids, respectively. We also showed that using the F relation from Ngeow et al. (2009), derived using only the LMC Cepheids, lead to the same IC 1613 distance within the uncertainties.

To take into account the possible change in the PL relations depending on metallicity, Tammann, Reindl, & Sandage (2011) derived new PL and period-color (PC) relations using the metal-poor Cepheids of the SMC from the OGLE-II database. The PL (and PC) relations of both F and FO pulsators seem

Table 4. Properties of the Candidate Variable Stars.

ID	Type[a]	R.A. (J2000)	Decl. (J2000)	$F475W$	$F814W$
VC01	MSV	09:59:15.90	+30:44:13.6	23.796	23.919
VC02	MSV	09:59:17.69	+30:44:54.6	25.232	25.222
VC03	MSV	09:59:18.88	+30:45:24.1	25.893	25.628
VC04	MSV	09:59:18.91	+30:45:27.6	24.400	24.473
VC05	LPV	09:59:21.05	+30:44:37.0	23.179	19.906
VC06	MSV	09:59:21.80	+30:45:19.8	24.688	24.756
VC07	ISV	09:59:22.20	+30:44:52.7	23.984	23.460
VC08	ISV	09:59:22.89	+30:45:53.1	24.420	23.314
VC09	LPV	09:59:23.02	+30:45:40.7	23.563	19.578
VC10	ISV	09:59:23.37	+30:46:01.6	23.696	23.090
VC11	MSV	09:59:23.38	+30:45:23.9	26.889	26.142
VC12	LPV	09:59:25.22	+30:45:23.7	22.076	19.164
VC13	MSV	09:59:26.37	+30:45:05.7	24.904	24.846
VC14	MSV	09:59:26.44	+30:45:01.9	22.518	22.696
VC15	MSV	09:59:26.56	+30:45:20.5	24.259	24.440
VC16	MSV	09:59:26.97	+30:44:30.1	25.619	25.642
VC17	MSV	09:59:27.50	+30:44:45.4	25.782	25.730
VC18	MSV	09:59:28.03	+30:44:17.4	22.496	22.721
VC19	MSV	09:59:28.52	+30:45:12.4	25.407	25.298
VC20	MSV	09:59:28.58	+30:45:59.0	26.000	25.905
VC21	MSV	09:59:28.60	+30:44:43.9	22.044	22.337
VC22	ISV	09:59:28.70	+30:45:46.0	22.394	21.565
VC23	MSV	09:59:29.16	+30:44:32.8	24.904	25.031
VC24	MSV	09:59:29.38	+30:44:59.3	23.763	23.970
VC25	MSV	09:59:29.40	+30:43:58.0	24.394	24.337
VC26	MSV	09:59:30.21	+30:44:41.2	20.776	20.823
VC27	MSV	09:59:30.43	+30:45:15.9	24.617	24.601
VC28	MSV	09:59:30.83	+30:44:19.5	22.807	23.045
VC29	ISV	09:59:30.94	+30:44:30.7	24.964	24.376
VC30	MSV	09:59:31.26	+30:44:41.6	23.431	23.613
VC31	MSV	09:59:31.78	+30:45:29.6	25.975	25.837
VC32	MSV	09:59:32.14	+30:45:05.1	27.136	26.730
VC33	MSV	09:59:32.26	+30:44:56.7	25.031	25.078

[a] ISV: instability strip variable; LPV: long period variable; MSV: main-sequence variable.

to present a break, so they fitted two linear regressions, treating the position of the break as a free parameter. For the F and FO Cepheids, they find the break at $\log P = 0.55$ and 0.40, respectively. A single F Cepheid of our sample has a period longer than the break, so we simply rejected it and used the PL relations for periods shorter than the breaks.

Finally, the PLC relation for SO Cepheids was derived by Bono, Caputo, & Marconi (2001) from their pulsational models. Due to the low amplitude of the SO light curves and very narrow instability strip, the uncertainties in distance are relatively small.

We note that the relations of Tammann, Reindl, & Sandage (2011) were calibrated assuming an SMC distance modulus of $(m-M)_{SMC,0}$=18.93, while those of Bono, Caputo, & Marconi (2001) applied to SMC Cepheids yielded $(m-M)_{SMC,0}$=19.11. For consistency with the distances determined in Paper II, we adapted the zero-points of these relations to give $(m-M)_{SMC,0}$=19.03.

Figure 11 summarizes the Cepheid-based distance calculations. The panels show the P−W_I (top) and P−M_I (middle) relations for F and FO Cepheids, and the PLC for SO Cepheids (bottom). The distance modulus obtained for each fit, corrected for foreground reddening (E(B−V)=0.021; Schlegel, Finkbeiner, & Davis 1998), is indicated in the top of each panel. We find that all the methods give values consistent with each other. A straight average of these measurements yield $(m-M)_{\rm Leo\ A,0}$ = 24.70, with a standard deviation of σ = 0.03. This is also in very good agreement with the Cepheid distance of Tammann, Reindl, & Sandage (2011), after taking into account the correction for the different assumed SMC distances.

Interestingly, while all the Cepheid-based distances agree with each other, they are somewhat longer than the distance obtained from the TRGB ($\Delta(m-M)_0 \sim 0.13$) and from the RR Lyrae stars ($\Delta(m-M)_0 \sim 0.18$). We do not believe this is an issue with the calibration from the *HST* flight system to the Johnson-Cousin system: as shown in Figure 8, even in the *HST* bands the Cepheids of Leo A are fainter than expected if the galaxy is located 0.1 mag further than IC 1613 as indicated by the difference in TRGB luminosity. Likewise, the luminosity of the Cepheid sample is unlikely to be biased toward fainter magnitudes due to the presence of a significant population of AC. The PL relations shown in Figure 11 are very tight, and apparently linear over the whole range of periods. Therefore, even if some AC are present in the sample, they are indistinguishable from the classical Cepheids and would not affect the distance measurements. This may indicate that the Cepheids in Leo A are intrinsically fainter at a given period than in the LMC, SMC, and IC 1613. This is discussed further in Section 8.2.

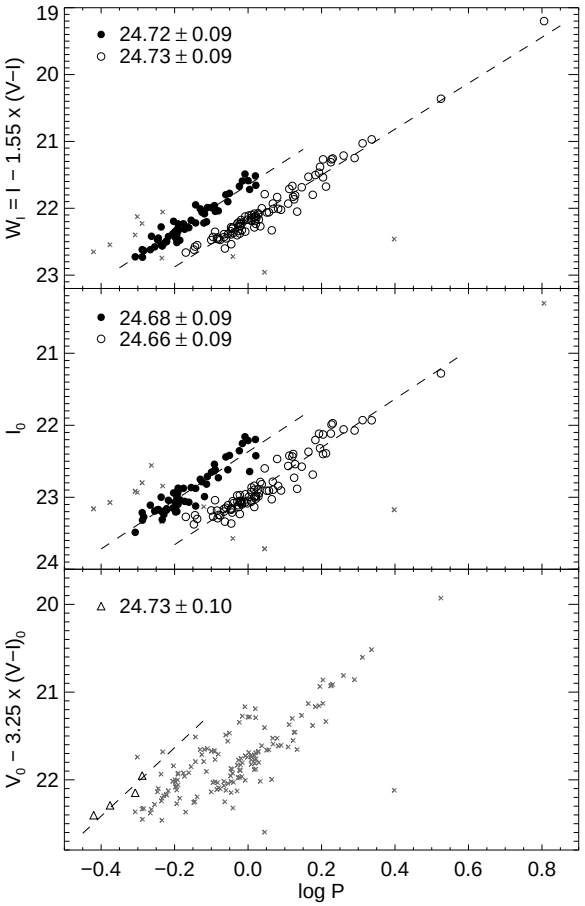

Figure 11. Period-luminosity diagrams for Cepheids in Leo A. The distance was determined using the P−W_I relations for F and FO Cepheids of Paper II (top), P−M_I relations for F and FO Cepheids of Tammann, Reindl, & Sandage (2011, middle), and the PLC for SO Cepheids from Bono, Caputo, & Marconi (2001, bottom). In each case, open circles, filled circles, and triangles show the F, FO, and SO Cepheids used for the fits, while the gray crosses represent the Cepheids that were rejected. The linear fits are shown as dashed lines, and the corresponding dereddened distance moduli are listed in the top of each panel.

8 DISCUSSION

8.1 Metallicity Evolution

We have calculated the distance to Leo A using several methods based on the properties of the Cepheids and RR Lyrae stars, as well as the luminosity of the TRGB. We find a good agreement between the values obtained from the TRGB and the RR Lyrae stars ($(m-M)_0$=24.57±0.13 and 24.48±0.12, respectively). These are also consistent with the recent literature value of $(m-M)_0 \sim 24.5$ (D02; Schulte-Ladbeck et al. 2002) obtained with similar methods.

The distance inferred from the RR Lyrae stars is quite sensitive to the metallicity adopted for these stars, which at the distance of Leo A cannot be directly measured. However, the SFH of Leo A calculated by Hidalgo et al. (2013, in preparation) from CMD-fitting provides the age-metallicity relation. It shows a very low metallicity at early times (Z∼0.0002, [Fe/H]∼ −2.0), followed by a steady metal enrichment until the present time when the metallicity derived is in fair agreement with the value inferred from H II regions.

The low metallicity for the old population is also required to explain several features of the observed CMD, such as the position of the HB and RC, and to obtain a good

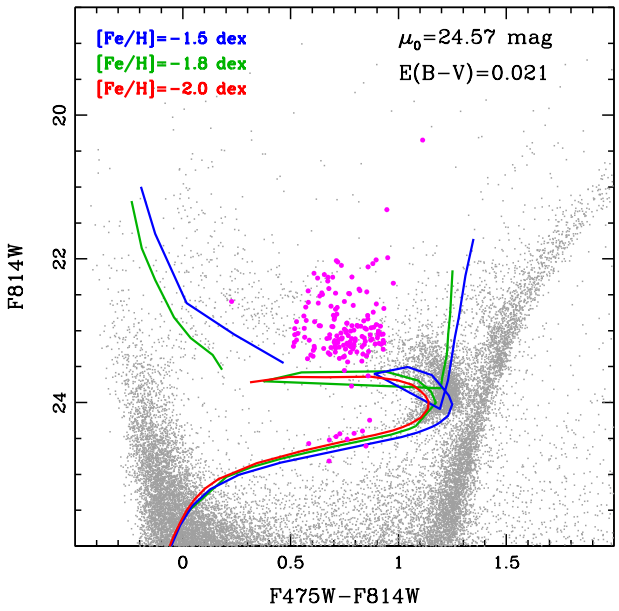

Figure 12. CMD showing the observed variable (magenta filled circles) and non-variable (gray dots) stars. Theoretical ZAHeBs are shown for three different metallicities. The lines at (F475W−F814W)∼0 indicate the maximum extent of the blue loops.

agreement between the observed HB and theoretical models. Close examination of the RC in Figure 7 reveals a thin, almost vertical group of stars at (F475W−F814W)∼1.1 and F814W∼24, slightly separated from the blue side of the RC. This suggests the presence of a small population of old stars, more metal-poor than the bulk of the RC stars.

To illustrate this, in Figure 12 we show the CMD of Leo A where theoretical ZAHeB of various metallicities have been overlain. The lines at (F475W−F814W)∼0 indicate the maximum extent of the blue loops. According to synthetic HB models in optical photometric bands, the ZAHeB locus is expected to be about 0.05 mag fainter than the lower envelope of the observed HB distribution (see Cassisi et al. 2004; Catelan 2004; Cassisi & Salaris 2013). This means that the best fit is provided by the [Fe/H]∼ −2.0 ZAHeB. At this metallicity, the ZAHeB also provides a very good fit to the "blue RC". On the other hand, the young stars of the blue loops are better represented by the higher metallicity, in agreement with the spectroscopic value of the H II regions. This suggests that the metallicity of Leo A has been increasing from [Fe/H]∼ −2 to [Fe/H]∼ −1.5 (i.e. a factor ∼3) over the past 10 Gyr or so.

8.2 Metallicity Dependence of the Cepheid PL Relation

The reason for the slightly longer distance obtained from the Cepheids (∼0.13) is not clear. Given the extremely low metallicity of Leo A it may also be explained by a metallicity effect, although the dependence on metallicity of the slopes and zero-points of PL relations is still debated (see, e.g., Sakai et al. 2004; Romaniello et al. 2008; Sandage, Tammann, & Reindl 2009; Storm et al. 2011). Figure 8 indicates that the Cepheids of Leo A are fainter than those in IC 1613, if we assume that the former are located 0.1 mag further than the latter as indicated by the difference in TRGB luminosity. Likewise, Figure 9 suggests that the shortest-period SMC Cepheids are, at a given period, slightly fainter than their more metal-rich LMC equivalent (see e.g. at log P ∼ −0.1). The luminosity difference between the short-period Cepheids of Leo A and the LMC is also significant. This may indicate that the luminosity of the short-period Cepheids decreases with decreasing metallicity, leading to a longer distance modulus than that obtained from the TRGB and the RR Lyrae stars.

In fact, such a trend with metallicity of the difference between the TRGB and Cepheid distances has been suggested before (Kennicutt et al. 1998; Sakai et al. 2004), in the sense that the distance modulus obtained from the Cepheids appeared increasingly longer than the TRGB distance modulus at decreasing metallicity. However, these results have recently been contested by Rizzi et al. (2007, see also Bono et al. 2008) who found no significant trend for the same sample of galaxies (see also Salaris & Cassisi 1998). While the origin of the discrepancy between the Sakai et al. (2004) and Rizzi et al. (2007) measurements is not discussed in the latter paper, it suggests that if the luminosity of the Cepheids does depend on metallicity the effect is smaller than the uncertainties currently affecting the measurements. For the sample of galaxies presented by Rizzi et al. (2007) – covering almost two orders of magnitude in nebular oxygen abundance – the difference between TRGB and Cepheid distance estimates has a standard deviation of 0.1, similar to the typical distance uncertainty to nearby galaxies.

The discrepancy between TRGB and Cepheid distances could also be unrelated to the stellar metallicity. Other possible factors affecting the distances obtained from Cepheids include the possible non-linearity of the PL relations (e.g. Ngeow et al. 2009), the intrinsic color of the Cepheids (Sandage & Tammann 2008), as well as the effects of stellar crowding and the properties of the intervening dust. Therefore, while the short-period Cepheids of Leo A appear to be intrinsically fainter than their equivalent in IC 1613 and the Magellanic Clouds, our data is not sufficient to conclusively claim the detection of a metallicity effect. On the other hand, the large number of Cepheids, combined with the fact that the metallicity of Leo A is significantly lower than any galaxy in the Rizzi et al. (2007) sample, make it a valuable galaxy when studying the metallicity dependencies of the variable star PL relationships.

9 SUMMARY AND CONCLUSIONS

We have analyzed time series HST/ACS data of the dIrr galaxy Leo A with the goal of searching for variable stars. Thanks to the significant depth of these data (i.e. >90 percent complete 2 mag below the HB), we have found 156 Cepheids and 10 RR Lyrae stars, as well as 33 candidate variables of various types. The number of RR Lyrae stars is very low compared to any other galaxies where these variables have been searched for, but is not unexpected given the insignificant fraction of old stars ($\gtrsim$8 Gyr) in this galaxy ($\lesssim$10 percent; Cole et al. 2007, S. Hidalgo et al. 2013, in preparation). The classification of Leo A in one of the Oost-

erhoff groups from the properties of its RR Lyrae stars is not settled: while the mean periods and number ratio clearly indicate a Oosterhoff type II – which is uncommon in Local Group galaxies – the location of these stars in the period-amplitude diagram suggests it is Oo-Intermediate. Follow-up data covering a larger FOV will be necessary to increase the sample.

The numerous Cepheids generally have very short periods, with the mode of the distributions at ∼1 and ∼0.6 day for F and FO pulsators, respectively. From their position on the PL diagram and light-curve morphology, we classify 91, 58, and 4 Cepheids as fundamental, first-overtone, and second-overtone mode CC, respectively, and two as population II Cepheids. We have showed, however, that some of the fainter CC may actually be AC; neither the sparse light curves nor their location in the PL diagrams allowed us to distinguish them convincingly.

We have calculated the distance to Leo A using the TRGB luminosity and various methods based on the photometric and pulsational properties of the Cepheids and RR Lyrae stars. Our best distance based on the TRGB method is $(m-M)_0 = 24.57\pm0.13$, corresponding to 820±50 kpc. This distance is in good agreement, within the uncertainties, with that obtained from the RR Lyrae stars ($(m-M)_0$=24.48±0.12) and literature values. The distance obtained from the Cepheid PL relations, however, is somewhat larger than these values, $(m-M)_0$=24.70±0.10. This may indicate that the short-period Cepheids of Leo A are intrinsically fainter than their equivalent in IC 1613 and the Magellanic Clouds. In any case, the very low metallicity of Leo A and its substantial populations of RGB stars, Cepheids, and RR Lyrae stars make it a valuable galaxy to investigate the possible metallicity dependencies of the variable star PL relationships.

Finally, while the current metallicity of Leo A is very low – the lowest within the star forming galaxies of the LG – the morphology of the HB and RC in the CMD require that it was even lower about 10 Gyr ago. This suggests that the metallicity of Leo A has increased from [Fe/H]∼ −2 to [Fe/H]∼ −1.5 (i.e. a factor ∼3) over the past 10 Gyr or so.

ACKNOWLEDGMENTS

The authors are grateful to the anonymous referee for thoughtful comments that helped improve the manuscript. Support for this work was provided by a rolling grant from the UK Science and Technology Facilities Council, the IAC (grants 310394 and P/301204), and the Education and Science Ministry of Spain (grants AYA2007-3E3506 and AYA2010-16717).

APPENDIX A: FINDING CHARTS

The finding charts for the whole sample of variable stars are presented in the electronic version of this paper (Figure A1).

REFERENCES

Bernard E. J., et al., 2009, ApJ, 699, 1742 (Paper I)
Bernard E. J., et al., 2010, ApJ, 712, 1259 (Paper II)
Bono G., Caputo F., Fiorentino G., Marconi M., Musella I., 2008, ApJ, 684, 102
Bono G., Caputo F., Marconi M., 2001, MNRAS, 325, 1353
Bono G., Caputo F., Marconi M., Musella I., 2010, ApJ, 715, 277
Bono G., Caputo F., Santolamazza P., Cassisi S., Piersimoni A., 1997, AJ, 113, 2209
Cacciari C., Corwin T. M., Carney B. W., 2005, AJ, 129, 267
Cassisi S., Castellani M., Caputo F., Castellani V., 2004, A&A, 426, 641
Cassisi S., Potekhin A. Y., Pietrinferni A., Catelan M., Salaris M., 2007, ApJ, 661, 1094
Cassisi, S., Salaris, M., 2013, Old Stellar Populations: How to Study the Fossil Record of Galaxy Formation. Wiley-VCH, Berlin, *in press*
Catelan M., 2009, Ap&SS, 320, 261
Catelan M., 2004, ApJ, 600, 409
Clementini, G., Gratton, R., Bragaglia, A., Carretta, E., Di Fabrizio, L., & Maio, M. 2003, AJ, 125, 1309
Cole A. A., et al., 2007, ApJ, 659, L17
Da Costa G. S., Armandroff T. E., 1990, AJ, 100, 162
Demarque P., Hirshfeld A. W., 1975, ApJ, 202, 346
Dolphin A. E., et al., 2001, ApJ, 550, 554
Dolphin A. E., et al., 2002, AJ, 123, 3154
Dolphin A. E., et al., 2003, AJ, 125, 1261
Fiorentino G., Limongi M., Caputo F., Marconi M., 2006, A&A, 460, 155
Fiorentino G., Stetson P. B., Bono G., Monelli M., Bernard E. J., Pietrinferni A., 2012, ApJ, 759, L12
Gallart C., Aparicio A., Freedman W. L., Madore B. F., Martínez-Delgado D., Stetson P. B., 2004, AJ, 127, 1486
Gössl C. A., 2007, PhD Thesis, Ludwig-Maximilians-Universität München, http://edoc.ub.uni-muenchen.de/7948/
Gössl C. A., Snigula J., Hopp U., 2006, in Walker A. R., Bono G., eds, Mem. S. A. It. Vol. 77, Stellar Pulsation and Evolution, p. 299
Gratton R. G., Bragaglia A., Clementini G., Carretta E., Di Fabrizio L., Maio M., Taribello E., 2004, A&A, 421, 937
Grevesse N., Noels A., 1993, in Prantzos N., Vangioni-Flam E., Cassé M., eds, Origin and Evolution of the Elements. Cambridge Univ. Press, Cambridge, p. 15
Harris W. E., 1996, AJ, 112, 1487
Hidalgo S. L., Aparicio A., Martínez-Delgado D., Gallart C., 2009, ApJ, 705, 704
Hoessel J. G., Saha A., Krist J., Danielson G. E., 1994, AJ, 108, 645
Horne J. H., Baliunas S. L., 1986, ApJ, 302, 757
Kennicutt R. C., Jr., et al., 1998, ApJ, 498, 181
Layden A. C., Ritter L. A., Welch D. L., Webb T. M. A., 1999, AJ, 117, 1313
Leavitt H. S., 1908, AnHar, 60, 87
Lee M. G., Freedman W. L., Madore B. F., 1993, ApJ, 417, 553
Monelli M., et al., 2010, ApJ, 720, 1225
Monelli M., et al., 2012, MNRAS, 422, 89
Ngeow, C.-C., Kanbur, S. M., Neilson, H. R., Nanthakumar, A., & Buonaccorsi, J. 2009, ApJ, 693, 691
Oosterhoff P. T., 1939, Obs, 62, 104
Pietrinferni, A., Cassisi, S., Salaris, M., & Castelli, F. 2004,

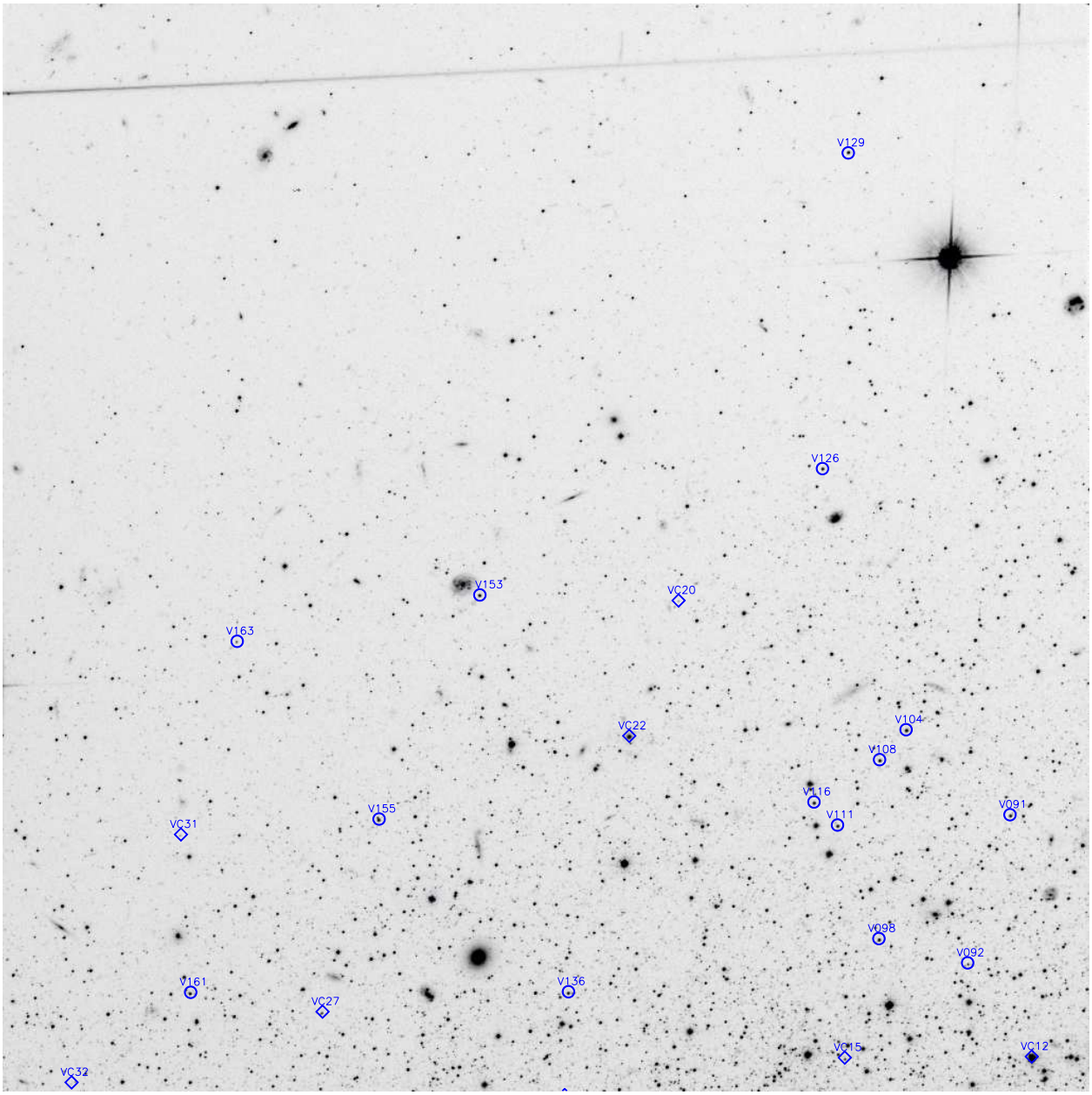

Figure A1. Finding chart for variables (circles) and candidate variables (diamonds) in the northeast quadrant. The full set of high-resolution finding charts is available as Supporting Information with the online version of the paper.

ApJ, 612, 168
Rizzi L., Tully R. B., Makarov D., Makarova L., Dolphin A. E., Sakai S., Shaya E. J., 2007, ApJ, 661, 815
Romaniello M., et al., 2008, A&A, 488, 731
Sakai S., Ferrarese L., Kennicutt R. C., Jr., Saha A., 2004, ApJ, 608, 42
Salaris M., 2012, Ap&SS, 341, 65
Salaris M., Cassisi S., 1998, MNRAS, 298, 166
Sandage A., 1986, AJ, 91, 496
Sandage A., Tammann G. A., 2008, ApJ, 686, 779
Sandage A., Tammann G. A., Reindl B., 2009, A&A, 493, 471
Schlegel D. J., Finkbeiner D. P., Davis M., 1998, ApJ, 500, 525
Schulte-Ladbeck R. E., Hopp U., Drozdovsky I. O., Greggio L., Crone M. M., 2002, AJ, 124, 896
Sirianni M., et al., 2005, PASP, 117, 1049
Skillman E. D., Kennicutt R. C., Hodge P. W., 1989, ApJ, 347, 875
Smith H. A., Catelan M., Clementini G., 2009, AIPC, 1170, 179
Snigula J., 2006, PhD Thesis, Ludwig-Maximilians-Universität München, http://edoc.ub.uni-muenchen.de/4980/
Soszyński I., et al., 2008a, AcA, 58, 163
Soszyński I., et al., 2008b, AcA, 58, 293
Soszyński I., et al., 2010a, AcA, 60, 17
Soszyński I., Udalski A., Szymański M. K., Kubiak M., Pietrzyński G., Wyrzykowski Ł., Ulaczyk K., Poleski R., 2010b, AcA, 60, 91

Stetson P. B., 1994, PASP, 106, 250
Storm J., Gieren W., Fouqué P., Barnes T. G., Soszyński I., Pietrzyński G., Nardetto N., Queloz D., 2011, A&A, 534, A95
Tammann G. A., Reindl B., Sandage A., 2011, A&A, 531, A134
Tolstoy E., et al., 1998, AJ, 116, 1244
Udalski, A., Soszyński, I., Szymański, M., Kubiak, M., Pietrzyński, G., Wozniak, P., & Zebrun, K. 1999a, Acta Astronomica, 49, 223
Udalski, A., Soszyński, I., Szymański, M., Kubiak, M., Pietrzyński, G., Wozniak, P., & Zebrun, K. 1999b, Acta Astronomica, 49, 437
Udalski, A., Szymański, M., Kubiak, M., Pietrzyński, G., Soszyński, I., Wozniak, P., & Zebrun, K. 1999c, Acta Astronomica, 49, 201
Vansevičius V., et al., 2004, ApJ, 611, L93
van Zee L., Skillman E. D., Haynes M. P., 2006, ApJ, 637, 269
Welch D. L., Stetson P. B., 1993, AJ, 105, 1813
Zwicky F., 1942, PhRv, 61, 489

Table A1. Cross-Identification with Previously Known Variables in Leo A.

ID	Period (days)	Type[a]	ID_{D02}	Period (days)	Type[b]	ID_{G07}	Period (days)	ID_{H94}	Period (days)
V002	0.935	F	C2-V24	0.47 ± 0.02	C-FO/SO	-	-	-	-
V004	0.934	F	C2-V55	0.94 ± 0.03	C	-	-	-	-
V005	1.63	F	C2-V39	1.69 ± 0.05	C-FM	LM53	2.674	-	-
V007	1.60	F	C2-V08	1.70 ± 9.99	C	-	-	-	-
V008	0.542	FO	C2-V27	0.55 ± 0.02	C-FO	-	-	-	-
V009	2.5	P2C	C2-V52	0.70 ± 0.06	C	-	-	-	-
V010	0.635	FO	C2-V20	0.65 ± 0.03	C-FO	-	-	-	-
V012	0.570	FO	C2-V03	0.60 ± 0.02	C	-	-	-	-
V013	1.343	F	C2-V23	1.52 ± 0.20	C-FM	-	-	-	-
V015	0.645	FO	C2-V21	0.64 ± 0.02	C	-	-	-	-
V017	0.643	FO	C2-V59	0.64 ± 0.02	C-FO	-	-	-	-
V021	1.82	F	-	-	-	LM04/LeoA-15	1.813	V13	3.41703
V023	0.627	FO	C2-V54	0.61 ± 0.01	C-FO	-	-	-	-
V024	0.947	FO	C2-V38	0.47 ± 0.02	C-SO	LL14	18.920	-	-
V025	1.40	F	C2-V37	1.28 ± 0.12	C-FM	LL11	57.912	-	-
V028	1.09	F	C2-V05	0.54 ± 0.02	C-FO	-	-	-	-
V029	0.587	*ab*	C2-V66	0.54 ± 0.03	RR	-	-	-	-
V031	1.327	F	C2-V25	1.39 ± 0.15	C-FM	LM10	4.008	V10	13.0040
V035	0.981	FO	-	-	-	LS01	0.981	V9	2.6704
V036	1.335	F	C2-V09	1.22 ± 0.18	C-FO	-	-	-	-
V037	1.525	F	-	-	-	LM17/LeoA-22	1.524	-	-
V038	0.871	F	C2-V49	0.86 ± 0.02	C-FM	-	-	-	-
V039	0.814	FO	C2-V19	0.82 ± 0.04	C-FO	-	-	-	-
V040	0.607	FO	C2-V26	0.61 ± 0.02	C-FO	-	-	-	-
V041	0.633	FO	C2-V13	0.64 ± 0.01	C-FO	-	-	-	-
V045	0.953	F	C2-V50	0.49 ± 0.01	C-FO	-	-	-	-
V053	1.08	F	-	-	-	LS39	0.188	-	-
V055	0.70	FO	C2-V34	0.68 ± 0.01	C-FO	-	-	-	-
V059	0.515	FO	-	-	-	LL02	65.446	-	-
V060	0.965	FO	-	-	-	LS26/LeoA-21	0.965	-	-
V061	2.170	F	-	-	-	LM16	2.164	-	-
V062	0.640	FO	C2-V61	0.64 ± 0.01	C-FO	-	-	-	-
V064	1.32	F	-	-	-	LM15	1.320	-	-
V067	3.35	F	-	-	-	LM03/V03/LeoA-11	3.354	-	-
V073	1.95	F	-	-	-	LM13	1.943	-	-
V082	1.57	F	C2-V43	1.61 ± 0.05	C-FM	LM39	1.562	-	-
V085	0.624	FO	C2-V53	0.63 ± 0.03	C	-	-	-	-
V088	1.56	F	-	-	-	LM07/V07/LeoA-9	1.564	V7	0.54837
V089	0.890	FO	-	-	-	LM54	8.390	-	-
V090	1.17	F	C2-V69	1.15 ± 0.04	C-FM	-	-	-	-
V093	1.60	F	C2-V42	1.73 ± 0.23	C-FO	LM02/V06/LeoA-20	1.607	-	-
V098	1.022	F	C2-V11	0.51 ± 0.01	C-SO	LM47	1.021	-	-
V100	0.516	FO	C2-V36	0.52 ± 0.02	C	-	-	-	-
V104	1.065	F	C2-V04	0.53 ± 0.02	C	-	-	-	-
V107	1.69	F	C2-V22	1.67 ± 0.13	C-FM	LM11	1.690	-	-
V111	0.90	F	C2-V07	0.87 ± 0.02	C	-	-	-	-
V114	1.46	F	C2-V31	1.46 ± 0.20	C-FM	-	-	-	-
V116	0.690	FO	C2-V06	0.68 ± 0.01	C-FO	-	-	-	-
V119	1.286	F	C2-V60	1.32 ± 0.11	C-FM	LM14	1.280	-	-
V122	0.810	FO	C2-V32	0.78 ± 0.04	C-FO	-	-	-	-
V124	1.687	F	-	-	-	LM09/V02	1.685	-	-
V126	0.983	F	-	-	-	LS35	0.450	-	-
V130	1.20	F	-	-	-	LM21	5.848	-	-
V135	6.394	F	-	-	-	LM01/V01/LeoA-5	6.490	-	-
V141	0.749	FO	C2-V30	0.75 ± 0.06	C-FO	-	-	-	-
V145	2.05	F	C2-V64	2.01 ± 9.99	C	LM06/V04	2.048	-	-
V147	0.813	F	C2-V46	0.60 ± 0.02	C-FO	-	-	-	-
V148	1.50	F	-	-	-	LM45	1.499	-	-
V153	0.652	FO	C2-V02	0.65 ± 0.02	C-FO	-	-	-	-
V155	0.775	FO	C2-V10	0.79 ± 0.04	C-FO	LS53	0.131	-	-
V157	1.68	F	C2-V58	1.46 ± 0.17	C-FM	LM05/V05	1.685	-	-
V158	1.052	F	-	-	-	LL05	10.391	-	-
V159	0.580	FO	C2-V48	0.59 ± 0.03	C-FO	-	-	-	-
V160	0.870	FO	-	-	-	LS29	0.465	-	-
V162	0.590	FO	C2-V35	0.39 ± 0.01	C-FO/SO	-	-	-	-
V164	0.667	FO	C2-V45	0.66 ± 0.02	C-FO	-	-	-	-
V165	0.795	FO	C2-V28	0.80 ± 0.04	C-FO	LM43	3.897	-	-
V166	0.586	FO	C2-V29	0.59 ± 0.02	C-FO	-	-	-	-
VC05	-	LPV	-	-	-	LeoA-14	170.70	V11	2.0064
VC09	-	LPV	-	-	-	LeoA-12	268.42	-	-
VC12	-	LPV	-	-	-	LeoA-10	919.28	-	-
VC30	-	MSV	-	-	-	LS56	0.269	-	-

[a] *ab*: fundamental mode RR Lyrae star; F, FO: fundamental mode and first-overtone Classical Cepheids; P2C: population II Cepheid; LPV: long period variable; MSV: main-sequence variable.
[b] Type from D02 – RR: RR Lyrae star; C-FM, C-FO, C-SO: fundamental mode, first-, and second-overtone Classical Cepheids; C: Cepheid of unknown type.